Polymer 50 (2009) 3887–3894

Contents lists available at ScienceDirect

Polymer

journal homepage: www.elsevier.com/locate/polymer

Synthesis and bulk organization of polymer nanocomposites based on hemi/ditelechelic poly(propylene oxide) end-functionalized with POSS cages

Solo Randriamahefa [a], Cédric Lorthioir [a,*], Philippe Guégan [b], Jacques Penelle [a]

[a] Equipe "Systèmes Polymères Complexes", Institut de Chimie et des Matériaux Paris-Est, Université Paris-Est and CNRS, 2-8 rue Henri Dunant, 94320 Thiais, France
[b] Laboratoire "Matériaux Polymères aux Interfaces", Université d'Evry – Val d'Essonne, Boulevard François Mitterrand, 91025 Evry Cedex, France

ARTICLE INFO

Article history:
Received 4 February 2009
Received in revised form
10 June 2009
Accepted 12 June 2009
Available online 21 June 2009

Keywords:
Chain end functionalization
POSS
Nanocomposites

ABSTRACT

A model hybrid material based on a molten and flexible polymer – atactic poly(propylene oxide) (PPO) – tethered with a monofunctionalized POSS molecule incorporated at one or both chain ends was synthesized. Asymmetric PPO chains with a hydroxyl terminal group were first allylated, using a Williamson ether synthesis. Hydrosilylation of the allyl end-functionalized PPO chains with hydro-heptacyclopentyl-substituted POSS cages resulted in the anchoring of a single POSS unit per allyl functionality. Two distinct PPO–POSS nanocomposites were prepared: one with a large fraction of PPO chains having two POSS end-groups; one made of a hemi-telechelic singly substituted PPO–POSS chain. Both architectures contained a similar POSS content. The influence of the number of POSS end-groups per chain on the bulk organization was investigated by wide-angle X-ray diffraction. For each nanocomposite, part of the POSS particles crystallize but a propensity to form larger crystalline regions is observed as the fraction of di-telechelic PPO–POSS chains increases. These variations in the bulk organization of the POSS cages within the molten PPO matrix influence the thermal oxidative degradation behavior of the polymer matrix, as evidenced by thermogravimetric analysis.

1. Introduction

Several types of Polyhedral OligoSilSesquioxane (POSS)-based polymer nanocomposites have been described over the last 15 years [1,2]. In addition to simple polymer/POSS physical blends [3,4], POSS units have been incorporated in statistical copolymers, one of the comonomers displaying the silsesquioxane cage either as a pendant side group (poly(methyl methacrylate), polystyrene, polyethylene or polypropylene backbone for instance) [5–10] or in the main chain (siloxane–silsesquioxane copolymers) [11]. POSS molecules have also been included as multifunctional cross-links in polymer networks [12,13] or as cores in star-like structures [14,15] (e.g., with poly(ethylene glycol) oligomers anchored at the eight corners of octahedral silsesquioxane cages [14]). Finally, homopolymer (poly(ethylene glycol) [16,17], polystyrene [18,19], poly(methyl methacrylate) [19–21], poly(ε-caprolactone) [22], poly(*N*-isopropylacrylamide) [23] or poly(acrylic acid) [24]) or copolymer (polyethylene-*b*-poly(ethylene oxide)) [25] chains with a POSS unit at a single or both chain ends have also been introduced.

All these polymeric systems display a common morphological feature, arising from the high propensity of the oligosilsesquioxane spheres to self-assemble into layered subunits. As a result, in polymers with high POSS contents, the inorganic particles associate in regular layered assemblies, giving rise to inorganic crystallites dispersed in the polymer matrix. In addition, a significant enhancement in the mechanical and thermodegradative properties is generally observed for these POSS-containing architectures in comparison to POSS-free polymer matrices. It is generally agreed upon that the molecular origin for the mechanical reinforcement of the polymer matrix is linked to the above morphological characteristics, although essential features to get a better understanding such as the influence of the POSS cages on the chain segment motions involved in the α-relaxation as well as the characteristic length scale over which the segmental dynamics is influenced by the POSS cages remain poorly understood.

In this contribution, a model experimental polymer system is introduced, aimed at casting further light on the molecular mechanisms at the basis of this mechanical effect. This model was designed to prevent the extra complexities and ambiguities associated with the interpretation of structure–property relationships in more complex systems such as those already described in the literature [10,13,26,27]. To reach this overall objective, a non-crystalline polymer with a sub-ambient glass-transition temperature –

* Corresponding author. Tel.: +33 1 49 78 13 08; fax: +33 1 49 78 12 08.
E-mail address: lorthioir@icmpe.cnrs.fr (C. Lorthioir).

0032-3861/$ – see front matter © 2009 Elsevier Ltd. All rights reserved.
doi:10.1016/j.polymer.2009.06.031

poly(propylene oxide) end-capped by a single POSS unit – was selected. This choice prevents the interference of alternate mechanisms that could otherwise affect the molecular motions of the polymer chain, e.g., the coexistence of competitive self-organizing mechanisms (joint crystallization of polymer chain and POSS units) or the dynamical heterogeneities of the segmental motions induced by the variations of the POSS location along the chains.

In this preliminary communication are presented the synthesis of a model hemi-telechelic poly(propylene oxide) (PPO), as well as corresponding thermal properties and morphological X-ray diffraction data.

2. Experimental section

2.1. Materials

Pentane (SDS) and allyl bromide (Acros) were dried over calcium hydride and distilled prior to use. Toluene (SDS) was distilled from sodium/benzophenone. Dimethylformamide (SDS) was dried over 3 Å molecular sieves under argon for 48 h and distilled. Commercial poly(propylene oxide) (PPO) homopolymers, PPO monobutyl ether (denoted as BuPPO; Aldrich; $M_n = 2850$ (degree of polymerization, DP = 49) as determined by ^{1}H NMR) and PPO monomethyl ether (denoted as MePPO; Polymer Source; $M_n = 3850$ (DP = 66) as determined by ^{1}H NMR), were dried at 50 °C under high vacuum for 24 h. 1-Hydrido-3,5,7,9,11,13,15-heptacyclopentyl-substituted polyhedral silsesquioxane (POSS; Aldrich; $M = 901.56$) was dried at 50 °C under high vacuum. Sodium hydride (60% dispersion in mineral oil, Aldrich) and Karstedt's catalyst ($C_8H_{18}OPtSi_2$, 2 wt% Pt solution in xylene; Aldrich) were used as-received.

Both PPO homopolymers are atactic and their microstructure was derived from the analysis of their ^{13}C NMR spectrum ($CDCl_3$, 100 MHz). The percentages of mm, mr + rm and rr triads are 26.6, 51.0 and 22.4%, respectively, for BuPPO and 25.8, 50.9 and 23.3%, respectively, for MePPO.

The structure and purity of 1-hydrido-3,5,7,9,11,13,15-heptacyclopentyl-substituted polyhedral silsesquioxane were checked by ^{1}H, ^{13}C and ^{29}Si NMR experiments. ^{1}H NMR ($CDCl_3$, 400 MHz): δ 4.14 (s, 1H, Si*H*); 1.76 (m, 14H, CH_2(Cp)), 1.59 (m, 14H, CH_2(Cp)), 1.50 (m, 28H, CH_2(Cp)); 1.00 (m, 7H, C*H*(Cp)); ^{13}C{^{1}H} NMR ($CDCl_3$, 100 MHz): δ 27.28, 27.25, 27.01, 26.96 (*C*H_2(Cp)), 22.20, 22.11 (*C*H(Cp)); ^{29}Si NMR ($CDCl_3$, 79 MHz): δ −66.47 (*Si*O_3CH(Cp)), −83.90 (*Si*HO_3).

2.2. Characterization and analysis

Size exclusion chromatography (SEC) measurements were carried out using a SHIMADZU LC10AD model pump, equipped with a RHEODYNE injector, two PLgel columns connected in series (PLgel 5 μm MIXED-C, Polymer Laboratories) and a refractive index detector (WYATT OPTILAB REX model). THF was used as the eluting solvent (flow rate: 1 mL min^{-1}) and the samples (concentration: 10 mg mL^{-1}) were injected at 20 °C. Molecular weights are reported relative to polystyrene standards.

NMR spectra were recorded in $CDCl_3$ on a Bruker Avance II spectrometer operating at 400 MHz (^{1}H), 100 MHz (^{13}C) and 75 MHz (^{29}Si) at ambient temperature.

Differential scanning calorimetry (DSC) measurements were carried out on a Perkin–Elmer Pyris Diamond calorimeter, equipped with an Intracooler III compressor, under nitrogen atmosphere. Samples were cooled to −85 °C at 100 °C min^{-1}, and subsequently heated to 60 °C at 10 °C min^{-1}. A second cooling-heating cycle was applied under the same conditions. The second heating scan showed a profile similar to the first one, thus ensuring that no sample degradation had occurred during the DSC experiment.

Thermogravimetric analysis (TGA) was performed using a Setaram Setsys Evolution 16 thermobalance under a controlled oxygen atmosphere (20 mL min^{-1}). The samples (approximate masses: 10–20 mg) were heated from room temperature to 700 °C at 10 °C min^{-1}.

Wide-angle X-ray powder diffraction data were collected at room temperature on a PANalytical X'Pert PRO MPD diffractometer operating in the reflection geometry, coupled with a fast detector (X'Celerator). Co Kα radiation ($\lambda = 1.79$ Å), induced by a generator operating at 40 kV and 30 mA, was used for the measurements. Diffraction patterns were recorded for 2θ-values ranging from 5° to 42°, with an angular increment of 0.02° and a counting time of 100 s.

2.3. Procedures

2.3.1. Synthesis of poly(propylene oxide) allyl ether

The procedure below describes the synthesis starting from the BuPPO homopolymer. A similar protocol was applied in the case of the MePPO homopolymer.

A 50 mL two-necked round-bottom flask equipped with a reflux condenser and a magnetic stirrer was charged with 1.0 g of crude NaH (dispersion in mineral oil) previously washed three times with pentane under argon flow. Dry BuPPO (1.34 g, 0.47 mmol) was dissolved in 8 mL dry DMF and added to the washed NaH via a cannula. The reaction mixture was stirred at room temperature overnight under argon. Dry allyl bromide (3 mL, 35 mmol) was then added via a syringe, and the mixture was stirred at 80 °C for 48 h under argon. Ethanol (2 mL) was added to quench the residual NaH. Water and dichloromethane were added to separate DMF, and after vigorous shaking, the two phases were separated. The organic phase was washed with water to remove any residual DMF. After removal of the solvent by evaporation and further drying under vacuum, 1.33 g of a colourless oil were obtained, corresponding to a 98% yield of allyl-functionalized poly(propylene oxide) chains denoted below as BuPPOallyl.

^{1}H NMR of BuPPOAllyl ($CDCl_3$, 400 MHz): δ (ppm) = 0.84 (t, C*H*$_3$–CH$_2$–CH$_2$–CH$_2$–); 1.07 (d, –CH$_2$–CH(C*H*$_3$)–O–); 1.30 (m, CH$_3$–C*H*$_2$–CH$_2$–CH$_2$–); 1.48 (m, CH$_3$–CH$_2$–C*H*$_2$–CH$_2$–); 3.33 (m, –CH$_2$–C*H*(CH$_3$)–O–); 3.48 (m, –C*H*$_2$–CH(CH$_3$)–O–); 3.94 (d, CH$_2$=CH–C*H*$_2$–O–CH$_2$–); 4.00 (d, –CH–O–C*H*$_2$–CH=CH$_2$); 5.09 and 5.20 (d, C*H*$_2$=CH–CH$_2$–); 5.84 (m, CH$_2$=C*H*–CH$_2$–).

^{1}H NMR of MePPOAllyl ($CDCl_3$, 400 MHz): δ (ppm) = 1.08 (d, –CH$_2$–CH(C*H*$_3$)–O–); 3.32 (s, C*H*$_3$–O–); 3.34 (m, –CH$_2$–C*H*(CH$_3$)–O–); 3.48 (m, –C*H*$_2$–CH(CH$_3$)–O–); 4.01 (d, CH$_2$=CH–C*H*$_2$–O–CH$_2$–); 5.08 and 5.20 (d, C*H*$_2$=CH–CH$_2$–); 5.85 (m, CH$_2$=C*H*–CH$_2$–).

2.3.2. Synthesis of telechelic poly(propylene oxide)–POSS

The procedure described below, using the BuPPOallyl homopolymer, was also applied when MePPOallyl was used as the starting material. The allyl-functionalized poly(propylene oxide) (BuPPOallyl; 694 mg; 0.24 mmol, allyl group: 0.36 mmol) and the POSS molecules (450 mg; 0.50 mmol) were dried in separate flasks at 50 °C under high vacuum for 24 h. The flasks were then filled with argon, and dry toluene (10 mL) was injected. The BuPPOallyl solution obtained was transferred via a cannula into the flask containing the POSS molecules. Karstedt's catalyst (12 μl) was added via a previously argon-purged syringe. The reaction mixture was stirred at 80 °C under argon for 18 h, then concentrated under vacuum. The obtained concentrated mixture was precipitated into a large amount of methanol, filtered and centrifuged to remove the unreacted POSS, which is insoluble in methanol. The product was dried under vacuum, and a 55% yield (0.58 g) of the isolated compound (BuPPO–POSS) was obtained.

^{1}H NMR of BuPPO–POSS ($CDCl_3$, 400 MHz): δ (ppm) = 0.59 (t, C*H*$_2$–Si); 0.98 (m, C*H*-cyclopentyl); 1.14 (d, –CH$_2$–CH(C*H*$_3$)–O–);

1.48, 1.57, 1.74 (m, CH_2-cyclopentyl); 3.40 (m, –CH_2–CH(CH_3)–O–); 3.55 (m, –CH_2–CH(CH_3)–O–).

^{1}H NMR of MePPO–POSS ($CDCl_3$, 400 MHz): δ (ppm) = 0.53 (t, CH_2–Si); 1.07 (d, –CH_2–CH(CH_3)–O–); 1.41, 1.51, 1.67 (m, CH_2-cyclopentyl); 3.33 (m, –CH_2–CH(CH_3)–O–); 3.48 (m, –CH_2–CH(CH_3)–O–).

3. Results and discussion

3.1. Synthesis and characterization of an n-butoxy-terminated PPO–POSS polymer contaminated by a disubstituted POSS–PPO–POSS polymer

A PPO homopolymer of low molecular weight, end-capped on one end by a POSS unit and on the other end by an *n*-butoxy ether, was synthesized according to the overall two-step reaction route described in Scheme 1. A hydroxy-terminated commercial PPO polymer, allegedly containing a butoxy end-group at the other extremity (BuPPO), was used as a precursor.

A ^{1}H NMR spectrum in $CDCl_3$ of this precursor evidenced the presence of a significant amount of polymer chains displaying other chain ends than the expected ones. In particular, ^{1}H NMR resonances assigned to allylic protons can be observed between 4 and 6 ppm (Fig. 1a). Such end-groups have been described previously in the literature, and have been attributed to a chain-transfer to monomer [28–30]. According to this literature, the strong basicity of the PPO propagating species induces a proton abstraction from the methyl group of propylene oxide, leading after rearrangement to allyl alcoholate, as depicted in Scheme 2. The formed alcoholate is nucleophilic enough to re-initiate a chain, but leads to unsaturated end-groups on the initiator side. In addition, the multiplet observed at 3.85 ppm on the ^{1}H NMR spectrum (Fig. 1a, peak i) can be assigned to the α proton of the hydroxyl end-group, –CH(CH_3)–OH. This signal is consistent with previous data reported by

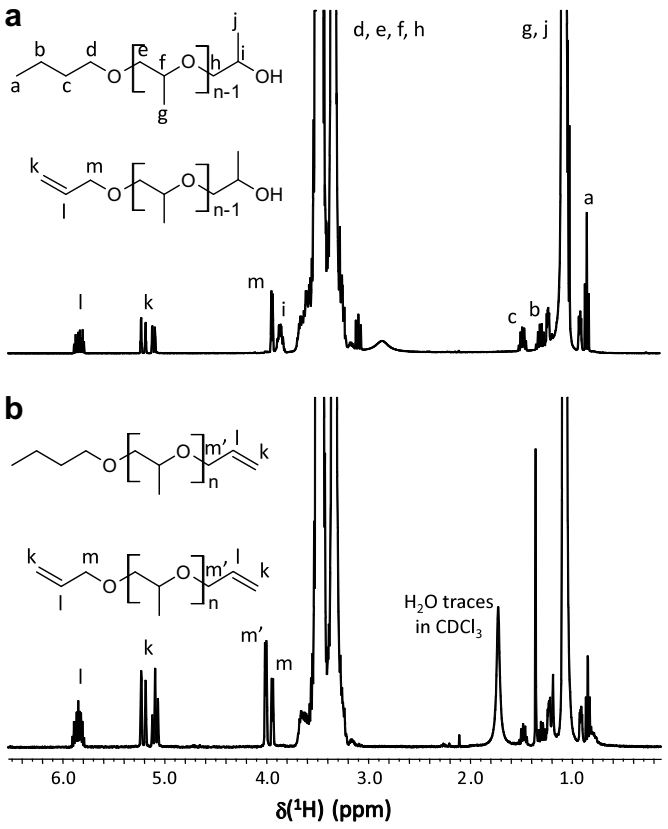

Fig. 1. ^{1}H NMR spectrum in $CDCl_3$ of: (a) the BuPPO homopolymer; (b) the BuPPO homopolymer after allylation of the hydroxyl terminal end-groups.

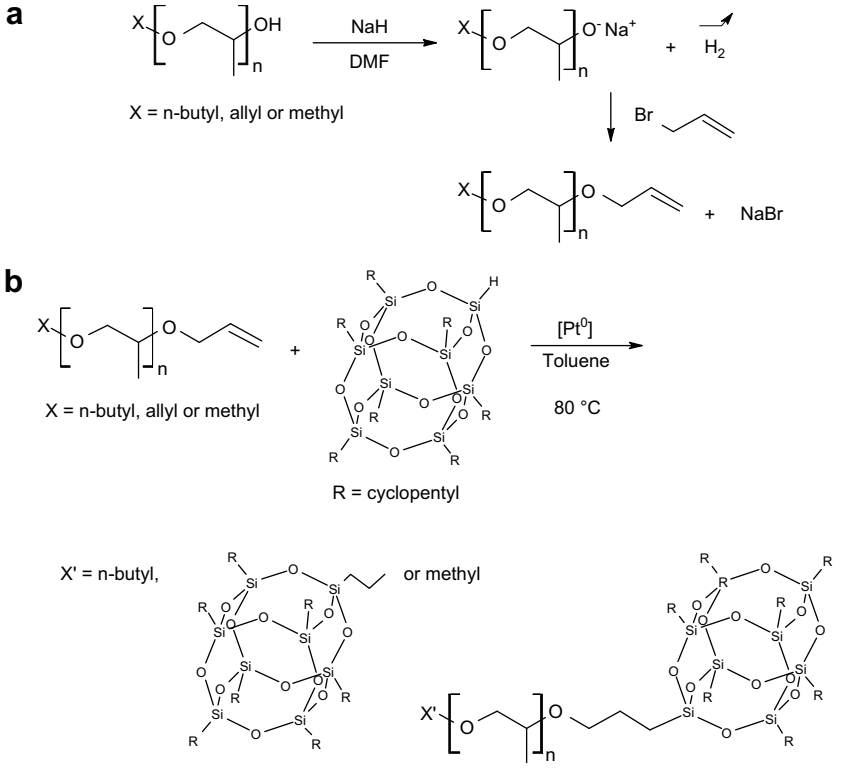

Scheme 1. (a) Preparation of the allyl-capped poly(propylene oxide) homopolymers and (b) their hydrosilylation with monofunctional POSS molecules.

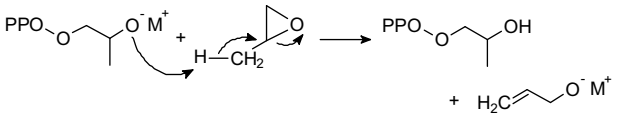

Scheme 2. Chain-transfer to monomer involved in the anionic polymerization of propylene oxide.

Brissault et al. [31], showing that the alcohol groups located at the chain ends of a similar commercial PPO homopolymer are mostly secondary hydroxyl groups.

A quantitative analysis of the ^{1}H NMR spectrum enabled the determination of a value of 0.95 ± 0.04 for the $(A_{Bu} + A_{allyl})/A_{CHOH}$ ratio, where A_{Bu} and A_{allyl} stand for the area per proton for the butyl CH_3 and the allyl CH_2 signals, respectively, while A_{CHOH} corresponds to the area under the resonance of the proton α to the secondary hydroxyl group. This ratio, very close to unity, suggests that the BuPPO homopolymer is mainly composed of chains displaying a hydroxyl terminal group at one end and either a butyl or an allyl group at the other extremity. The amount of putative α, ω-dihydroxy-terminated PPO chains can be considered negligible. Moreover, the proportion of chains containing allyl groups as chain ends is rather significant, since it amounts to about 64% of the BuPPO chains, as deduced from the ^{1}H NMR data. The remaining fraction corresponds to butoxy-terminated chains.

A number-average degree of polymerization of 48 can be determined according to the following equation: $DP = A_{CH3}[3(A_{Bu} + A_{allyl})]^{-1}$, where A_{CH3} accounts for the area under the resonance of the PPO methyl protons. This number corresponds to a realistic M_n value of 2.85×10^3.

The terminal hydroxyl groups of the characterized BuPPO homopolymer were converted into allylic ethers, using a one-pot two-step procedure. First, a PPO alcoholate was generated by adding sodium hydride in dry DMF, under inert atmosphere and at room temperature. In a second step, the formed alcoholate was reacted with allyl bromide at 80 °C for 24 h, according to a Williamson-type ether synthesis whose conditions had been used by Lestel et al. [32,33] and Brissault et al. [31] to prepare α,ω-diallyl-poly(ethylene oxide) and α,ω-diallyl-PPO, respectively. In spite of the low reactivity of the secondary hydroxyl group, a quantitative conversion for the allylation of the PPO homopolymers was observed by ^{1}H NMR (Fig. 1b): the α proton resonance peak of the hydroxyl terminal groups at 3.85 ppm has fully disappeared. In addition, the OH resonance peak previously observed in a ^{1}H NMR spectrum recorded in DMSO has also disappeared (see Figs. S1–S3, Supporting information).

The initially present allyl groups can be distinguished from those produced by the etherification reaction. The first type of allyl groups are characterized by CH_2 allyl protons bonded to the methyleneoxy group (–O–CH_2–$CH(CH_3)$–) on the terminal PPO repeat unit, with a ^{1}H NMR peak at 3.94 ppm. In contrast, the second type of allyl groups involve CH_2 allyl protons bonded to the –$OCH(CH_3)$– group of the terminal PPO repeat unit, with a corresponding ^{1}H NMR peak located at 4.00 ppm. The ratio between the areas under these peaks provides an estimate for the percentage of the α,ω-diallyl-PPO chains in the allylated BuPPO (BuPPOallyl). This proportion amounts to 64%, which is in full agreement with the percentage of allyl end-capped chains determined in the initial BuPPO precursor. After allylation, all the PPO chains display at least one allyl terminal group. As a result, the ^{1}H NMR peak assigned at 4.00 ppm can be used to recalculate the degree of polymerization. Using the resonance of the PPO methyl protons, a DP value of 48 is found. This value is, given the accuracy of a ^{1}H NMR quantitative analysis, similar to the one previously calculated on the initial BuPPO homopolymer, thus confirming the assumption made on the BuPPO chain ends and their distribution.

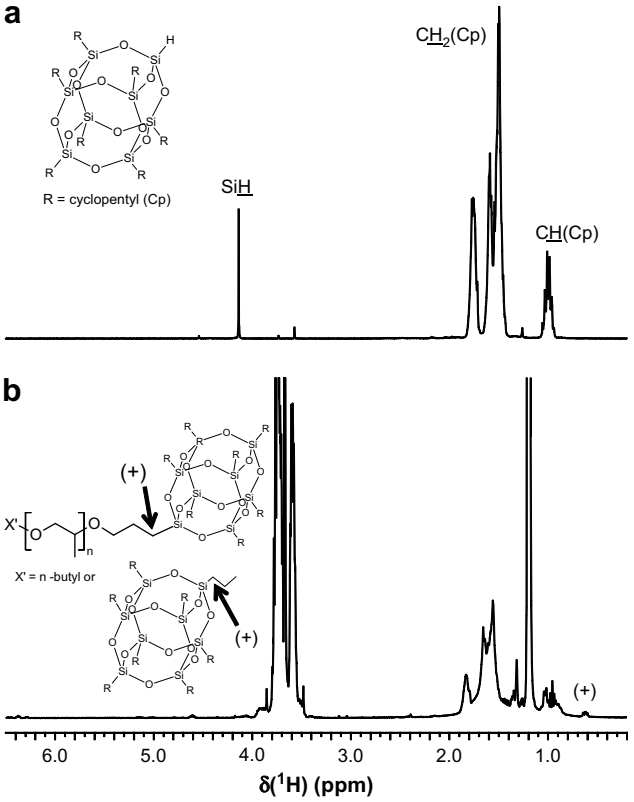

Fig. 2. ^{1}H NMR spectrum in $CDCl_3$ of: (a) the 1-hydrido-3,5,7,9,11,13,15-heptacyclopentyl-substituted POSS units; (b) the BuPPO chains with POSS cages grafted at either one (36 mol%) or both (64 mol%) chain ends.

A hydrosilylation reaction on the C=C double bond of the allylic end-groups was used to add the POSS molecules to the allyl-modified BuPPO polymer (Scheme 1b). An octahedral POSS cage with a single Si–H group and seven inert cyclopentyl groups was selected to prevent cross-linking reactions. Karstedt's platinum-based catalyst was chosen to catalyze the reaction. As expected, the ^{1}H NMR spectrum of the reaction product displays an additional proton resonance peak at 0.59 ppm, which can be assigned to the Si–CH_2 protons (Fig. 2). Moreover, the peaks related to the allyl protons disappear, as can be seen in Fig. 2b. After hydrosilylation, α,ω-diallyl- and monoallyl-PPO chains lead to α,ω-POSS-difunctionalized and POSS-monofunctionalized PPO chains, respectively. The relative amount between hemi- and di-telechelic PPO–POSS chains remains the same as the one between α,ω-diallyl- and monoallyl-PPO chains in BuPPOallyl, namely 64%/36%. Finally, unreacted POSS cages cannot be detected by ^{1}H NMR (no SiH signal at 4.1 ppm in Fig. 2b).

In general, a hydrosilylation reaction leads to α- and β-additions to the double bond, leading to Si–$CH(CH_3)$– groups and Si–CH_2– groups, respectively. For platinum-catalyzed hydrosilylation however, anti-Markovnikov addition, i.e. a β-addition, is usually observed [34]. A comparison between the areas of the SiCH_2 proton peak and the POSS cyclopentyl CH_2 proton peak suggests that the β-addition is predominant as expected. It should be noted that an accurate quantitative determination of the cyclopentyl CH_2 contribution is made difficult by an overlap with the CH_2 protons of the butyl chain ends (peak c, Fig. 1).

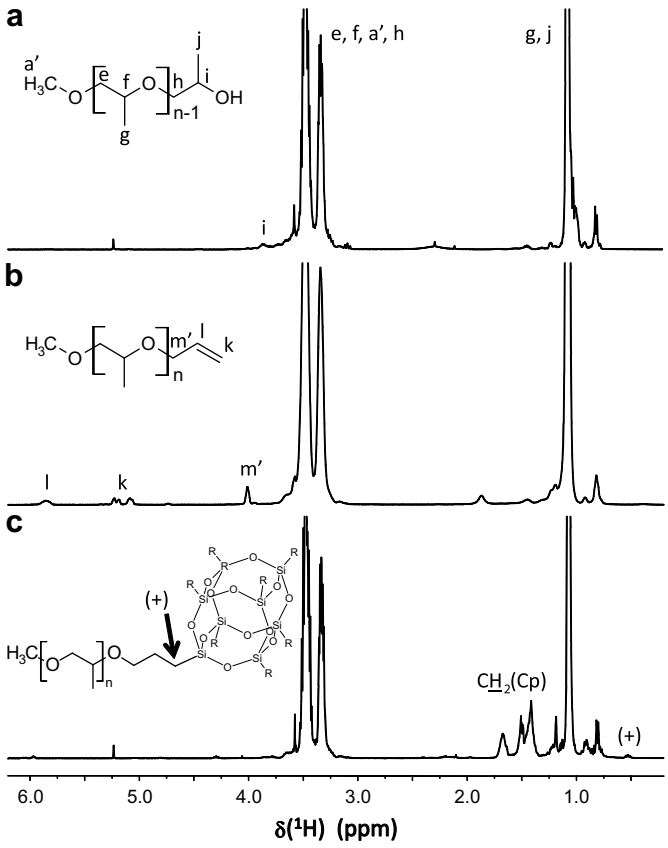

Fig. 3. ^{1}H NMR spectrum in $CDCl_3$ of: (a) the asymmetric MePPO homopolymer; (b) the allylated MePPO; (c) the MePPO–POSS hemi-telechelic hybrid.

3.2. Synthesis and characterization of a structurally pure methoxy-terminated PPO–POSS polymer

The previous experiments demonstrated that a well-characterized mixture of POSS-monofunctionalized (36%) and α,ω-POSS-difunctionalized (64%) PPO chains can be obtained from a commercial PPO polymer. In order to obtain an "uncontaminated" PPO chain terminated by a single POSS unit, a supposedly pure PPO precursor characterized by a methoxy group at one end and a hydroxyl group at the other extremity (MePPO) was considered. No allyl groups were detected for this PPO homopolymer, as evidenced by ^{1}H NMR experiments (Fig. 3a). This is due to the fact that the precursor was synthesized by anionic polymerization of propylene oxide using a combination of sodium 2-methoxyethoxide and triisobutylaluminium as initiator [35]. The addition of trialkylaluminium to the alkali metal alkoxide/PPO system in hydrocarbon media is known to increase the polymerization rate and reduces monomer chain-transfer, thus limiting the amount of allyl chain ends [30].

The procedure applied to the BuPPO homopolymer was also applied to MePPO, and again, a complete conversion of the terminal hydroxyl groups into allyl chain ends was observed (see Fig. 3b). The ^{1}H NMR spectrum of the reaction product obtained after hydrosilylation does not display the characteristic resonance assigned to the SiH proton ($\delta = 4.10$ ppm) as can be seen in Fig. 3c. Besides, the peak areas corresponding to the Si–CH_2 protons at 0.53 ppm and the POSS cyclopentyl CH_2 protons between 1.40 and 1.80 ppm lead to a relative ratio of about 2/56, as expected. This result indicates a total anchoring of POSS derivatives to the allylic functions of the modified PPO. These spectroscopic data are consistent with SEC results, which display an increase in the M_n value of about 1.0×10^3, a preserved monomodal distribution and an unmodified M_w/M_n value of 1.5, as shown in Fig. 4.

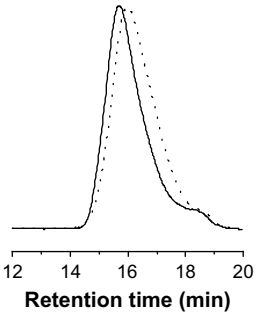

Fig. 4. SEC chromatograms of the starting MePPO homopolymer (dotted line) and the MePPO–POSS hybrid (solid line).

3.3. Bulk organization of the PPO–POSS nanocomposites

The POSS filler content was first determined using the ^{1}H NMR spectra of the BuPPO–POSS and MePPO–POSS nanocomposites. A comparison of the peaks at 1.48 and 1.57 ppm, assigned to the CH_2 protons of the POSS cyclopentyl groups, with the peak related to the PPO methyl protons shows that the POSS weight fraction in

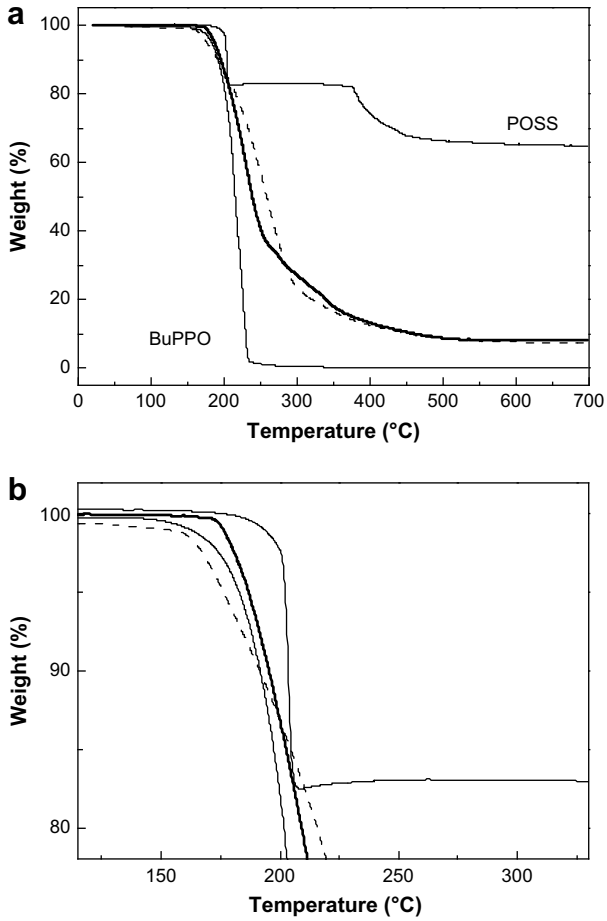

Fig. 5. (a) Thermogravimetric analysis of the BuPPO–POSS (thick solid line) and MePPO–POSS (dashed line) nanocomposite structures carried out in air at a heating rate of 10 °C min^{-1}. The TGA traces obtained under the same conditions with neat BuPPO and POSS are also displayed (thin solid lines). (b) Expansion of Fig. 5a between 115 °C and 330 °C.

BuPPO–POSS amounts to about 12.7 wt%. A similar value (13.0 wt%) was obtained for the MePPO–POSS hybrid materials.

The thermal stability of the PPO–POSS nanocomposites was investigated by TGA. Fig. 5 depicts the thermograms of BuPPO–POSS and MePPO–POSS in air. The individual components – BuPPO and neat POSS – are also included for comparison. The thermal oxidative degradation of the BuPPO homopolymer occurs over a rather narrow temperature range, with an onset of decomposition at 140 °C. At about 265 °C, the weight loss is quantitative. Interestingly, the TGA trace recorded on the BuPPO–POSS hybrid material shows that the onset of PPO decomposition is higher by about 30 °C and that the degradation rate of the polymer matrix in this nanocomposite structure is significantly lowered. Although the upper value of the corresponding temperature range of PPO degradation is difficult to determine due to the contribution from the second step of POSS decomposition, an increase of at least 110 °C, in comparison to neat BuPPO, is observed. Finally, assuming a similar thermo-oxidative decomposition mechanism for POSS units in neat POSS and in the PPO–POSS nanocomposites, the filler loading of BuPPO–POSS estimated by ^{1}H NMR leads to an expected char yield of about 8.26 wt%, in very good agreement with the experimental char yield (Fig. 5). Moreover, similar char yield values are obtained for both PPO–POSS nanocomposites, in agreement with the similar POSS weight fractions in the BuPPO–POSS and MePPO–POSS materials as determined by ^{1}H NMR. Differences can be observed between the thermal behavior of both PPO–POSS nanocomposites, although the corresponding TGA traces are qualitatively similar. In the case of MePPO–POSS, the onset of decomposition is found to be equal to 145 °C, corresponding within experimental error to the degradation temperature of neat PPO. The onset of decomposition occurs at a lower temperature for MePPO–POSS than for BuPPO–POSS. However, a significantly weaker weight loss is detected for MePPO–POSS than for BuPPO–POSS between 200 and 285 °C. Such differences might result from a distinct bulk organization in both PPO–POSS nanocomposites, in spite of their similar filler content. The organization of the POSS cages in these nanocomposites was thus investigated by WAXS.

The diffraction pattern obtained on the BuPPO–POSS hybrid material is reported in Fig. 6. The X-ray diffractograms recorded for a neat POSS, as well as for a PPO/POSS physical mixture at identical filler loading, are also included for the sake of comparison. The diffraction pattern of neat POSS displays sharp Bragg peaks, with a half-height angular width $\Delta(2\theta)$ of 0.24° for the peak at $2\theta = 9.45°$. On the diffractogram of BuPPO–POSS, in the range of 2θ values considered (Fig. 6a), two Bragg diffraction peaks are observed at $2\theta = 9.76°$ and 37.20°, in addition to the amorphous halo related to the amorphous PPO chains. This result indicates the presence of POSS crystallites within the amorphous PPO matrix. These peaks result from crystallites containing POSS molecules exclusively grafted to PPO chains as the ^{1}H NMR experiments on this hybrid material had indicated the absence of free POSS cages. As previously suggested by Zheng et al. [36,37], the anchoring of POSS molecules to polymer chains inhibits the growth of POSS crystallites, in the direction occupied by the PPO chains, leading to a 1D or 2D crystalline organization of the POSS units. Such an organization would lead to three-dimensional structures corresponding to columnar or lamellar POSS-based structures, with the anchored PPO chains surrounding these POSS assemblies. Of course, the occurrence of more complex shapes of the POSS crystallites cannot be discarded. The diffraction peaks detected on BuPPO–POSS remain rather narrow, with a half-height angular width of about $\Delta(2\theta) = 0.41°$ for the peak at $2\theta = 9.76°$. Using the Scherrer equation, the apparent size of the POSS crystallites within the BuPPO–POSS nanocomposite may be roughly estimated to about 25 nm. This value indicates that the POSS crystallites observed in BuPPO–POSS are somehow

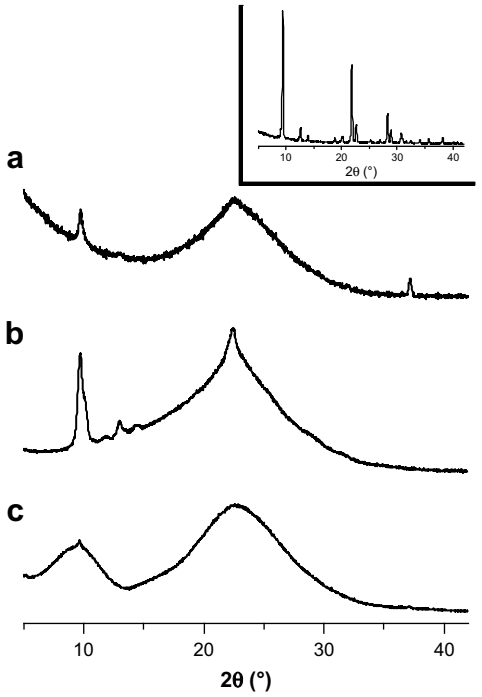

Fig. 6. X-ray diffractograms obtained on: (a) the BuPPO–POSS nanocomposite; (b) a BuPPO/POSS physical blend characterized by the same POSS weight fraction as BuPPO–POSS (12.7 wt%); (c) the MePPO–POSS nanocomposite (POSS content: 13.0 wt%). Inset: X-ray diffractogram of the neat 1-hydrido-3,5,7,9,11,13,15-heptacyclopentyl-substituted POSS.

extended, although their characteristic size is reduced compared to the one involved in neat POSS. The diffraction pattern obtained on the PPO/POSS physical blend is displayed in Fig. 6b. The ratio of the areas under the Bragg diffraction peak at $2\theta = 9.76°$ and under the PPO amorphous halo is about 4 times smaller for BuPPO–POSS than for the physical mixture. This feature suggests that in the BuPPO–POSS nanocomposite, all the POSS cages are not involved in crystalline domains, implying the occurrence of isolated POSS molecular chain ends or small disordered POSS aggregates as schematically depicted in Fig. 7. When comparing these data with the diffractogram recorded on MePPO–POSS depicted in Fig. 6c, one can notice that the shape of the peak occurring around 9–10° differs significantly from the narrow Bragg diffraction peak detected in the BuPPO–POSS nanocomposite. In the case of MePPO–POSS, a weak narrow contribution superimposes to a broad one. Such a behavior may be induced by the coexistence of a small amount of POSS crystallites characterized by a significant characteristic size (similar to the typical size of the crystallites observed for BuPPO–POSS) with a large portion of POSS crystallites displaying a highly reduced size.

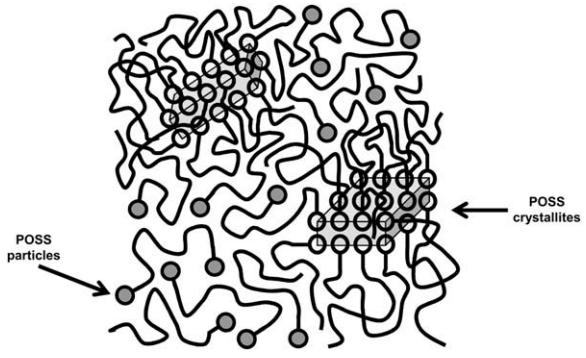

Fig. 7. Schematic representation of BuPPO–POSS in the bulk state.

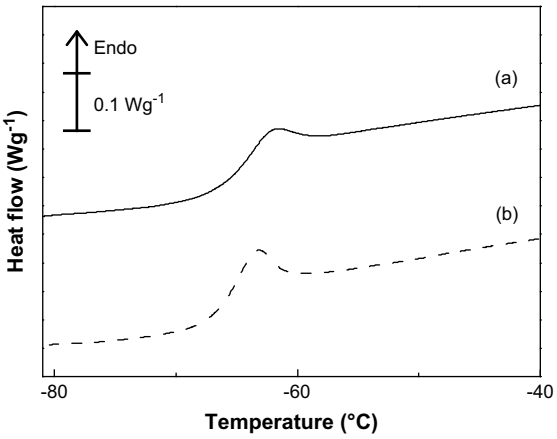

Fig. 8. DSC thermograms recorded on (a) the BuPPO–POSS nanocomposite and (b) the BuPPO homopolymer during a heating scan carried out at 10 °C min^{-1}. The samples were previously cooled to −85 °C from the molten state, with a cooling rate of 100 °C min^{-1}.

It must be noted that the same procedure was applied during the synthesis of both PPO–POSS nanocomposites, including a similar rate of solvent evaporation. Therefore, taking into account that BuPPO–POSS corresponds to a mixture of ditelechelic (64 mol%) and hemi-telechelic (36 mol%) PPO–POSS chains while MePPO–POSS involves POSS-monofunctionalized PPO chains only, the differences observed between the diffractograms of BuPPO–POSS and MePPO–POSS might indicate that the POSS crystallization process becomes easier as the amount of PPO chains tethered by a POSS cage at both chain ends increases.

The glass-transition temperature (T_g) as well as the width of the glass-transition (ΔT_g) measured for the PPO chains in the BuPPO–POSS nanocomposite are very similar to the ones measured for the initial BuPPO homopolymer, as shown in Fig. 8. A small increase of at most 1–2 °C is observed for the T_g value of the PPO chains in BuPPO–POSS, but this difference lies in the range of the experimental accuracy. In the case of the MePPO–POSS hybrid material, the T_g value is identical to the T_g of the MePPO homopolymer. Such results are in agreement with previous observations by Cardoen et al. on polystyrene (PS) chains functionalized by a POSS molecule at a single chain extremity [18]. In this work, an increase in the T_g value was observed for a molecular weight corresponding to about 8 PS repeat units while no variation was detected for polymerization degrees higher than 20.

In the MePPO–POSS nanocomposite, each PPO chain is anchored by one of its ends to a POSS cage possibly involved in POSS crystallites. Thus, the segmental dynamics of the first repeat units along the PPO chains, located close to the junction with the POSS cage, should be slowed down compared to the units in the middle of the chains. In the present case, the PPO molecular weight is too high to affect the segmental mobility of a significant part of the PPO repeat units and to induce a shift in the T_g value. It is expected that the restriction in the segmental mobility should be more pronounced for the PPO chains functionalized by a POSS unit at each chain end. In the BuPPO–POSS nanocomposite, about 64% of such chains are mixed with 36% of POSS monofunctionalized PPO chains, which should display, comparatively, a higher segmental mobility and induce a plasticizing effect. This feature might be responsible for the absence of a significant variation in the PPO T_g.

4. Conclusions

Organic/inorganic hybrid materials were synthesized, based on poly(propylene oxide) (PPO) chains tethered with monofunctionalized POSS molecules incorporated at a single or at both chain ends. PPO homopolymers were first end-functionalized by allyl groups, using a Williamson ether synthesis. A hydrosilylation reaction of the allylated PPO chains with 1-hydrido-3,5,7,9,11,13,15-heptacyclopentyl-substituted POSS cages enabled to anchor one chain end per POSS molecule. In the present study, two extreme cases of starting PPO homopolymers were considered: one composed of a dominant proportion of chains displaying an allyl terminal group (64 mol%) and another one obtained using synthetic procedures limiting the chain-transfer process, thus characterized by a negligible amount of allyl chain ends. The first PPO homopolymer led to a well-characterized mixture of PPO chains tethered at a single (36 mol%) or at both (64 mol%) extremities by a POSS molecule. The second PPO homopolymer yielded hemi-telechelic PPO–POSS chains.

Both synthesized PPO–POSS nanocomposites were characterized by a similar POSS content of about 13.0 wt%. The occurrence of POSS molecular chain ends induces a significant enhancement of the PPO thermal stability in air. Depending on the proportion of hemi-/di-telechelic PPO–POSS chains, variations in the thermal oxidative PPO degradation behavior are observed. Such a feature may result from the distinct bulk organization of the POSS cages within the amorphous PPO matrix. Indeed, in both nanocomposite structures, domains composed by isolated POSS particles anchored to a PPO chain coexist with regions containing self-assembled POSS particles, giving rise to crystallites. However, the characteristic POSS crystallite size is, on average, much higher in the hybrid material characterized by a large content of PPO chains tethered by POSS cages at both chain ends. This architecture seems to promote POSS crystallization, in comparison to the hemi-telechelic PPO–POSS structure.

Finally, no variation in the glass-transition of bulk PPO chains in both PPO–POSS nanocomposites could be detected by DSC. The PPO chain length is probably too high to detect polymer/filler interfacial phenomena. 2D solid-state NMR experiments on these model systems are currently under way and will be reported soon. They should open the way to a selective description of the segmental motions displayed by the PPO repeat units located close to the POSS cages. Such data on the gradient of chain mobility induced by the POSS units would lead to a deeper understanding of the role that they play in the enhancement of the mechanical properties usually observed in many POSS-based nanocomposites.

Acknowledgments

The authors gratefully acknowledge the French National Agency for Research (ANR) for financial support (ANR JC05_45573 COPOLYPOSS grant). CL thanks Professor Françoise Lauprêtre for helpful discussions.

Appendix. Supporting information

Supplementary data associated with this article (^{1}H NMR spectra in DMSO for both BuPPO and allylated BuPPO homopolymers) can be found in the online version at doi:10.1016/j.polymer.2009.06.031.

References

[1] Phillips SH, Haddad TS, Tomczak SJ. Curr Opin Solid State Mater Sci 2004;8(1):21–9.
[2] Wu J, Mather PT. Polym Rev 2009;49(1):25–63.
[3] Bian Y, Pejanović S, Kenny J, Mijović J. Macromolecules 2007;40(17):6239–48.
[4] Hao N, Böhning M, Schönhals A. Macromolecules 2007;40(26):9672–9.
[5] Lichtenhan JD, Otonari YA, Carr MJ. Macromolecules 1995;28(24):8435–7.
[6] Haddad TS, Lichtenhan JD. Macromolecules 1996;29(22):7302–4.
[7] Pyun J, Matyjaszewski K. Macromolecules 2000;33(1):217–20.
[8] Zheng L, Farris RJ, Coughlin EB. Macromolecules 2001;34(23):8034–9.

[9] Zheng L, Rajeswari MK, Farris RJ, Coughlin EB. J Polym Sci Part B Polym Phys 2002;40(9):885–91.
[10] Fu BX, Lee A, Haddad TS. Macromolecules 2004;37(14):5211–8.
[11] Lichtenhan JD, Vu NQ, Carter JA, Gilman JW, Feher FJ. Macromolecules 1993;26(8):2141–2.
[12] Matějka L, Strachota A, Pleštil J, Whelan P, Steinhart M, Šlouf M. Macromolecules 2004;37(25):9449–56.
[13] Bian Y, Mijović J. Macromolecules 2008;41(19):7122–30.
[14] Markovic E, Ginic-Markovic M, Clarke S, Matisons J, Hussain M, Simon GP. Macromolecules 2007;40(8):2694–701.
[15] Pan Q, Gao L, Chen X, Fan X, Zhou Q. Macromolecules 2007;40(14):4887–94.
[16] Kim BS, Mather PT. Macromolecules 2002;35(22):8378–84.
[17] Lee W, Ni S, Deng J, Kim BS, Satija SK, Mather PT, et al. Macromolecules 2007;40(3):682–8.
[18] Cardoen G, Coughlin EB. Macromolecules 2004;37(13):5123–6.
[19] Ohno K, Sugiyama S, Koh K, Tsujii Y, Fukuda T, Yamahiro M, et al. Macromolecules 2004;37(23):8517–22.
[20] Koh K, Sugiyama S, Morinaga T, Ohno K, Tsujii Y, Fukuda T, et al. Macromolecules 2005;38(4):1264–70.
[21] Huang CF, Kuo SW, Lin FJ, Huang WJ, Wang CF, Chen WY, et al. Macromolecules 2006;39(1):300–8.
[22] Ni Y, Zheng S. Macromolecules 2007;40(19):7009–18.
[23] Zhang W, Liu L, Zhuang X, Li X, Bai J, Chen Y. J Polym Sci Part A Polym Chem 2008;46(21):7049–61.
[24] Zhang W, Fang B, Walther A, Müller AHE. Macromolecules 2009;42(7):2563–9.
[25] Miao J, Cui L, Lau HP, Mather PT, Zhu L. Macromolecules 2007;40(15):5460–70.
[26] Brus J, Urbanová M, Strachota A. Macromolecules 2008;41(2):372–86.
[27] Pitard D. PhD thesis, University Paris XII, Créteil, France; 2008.
[28] St Pierre LE, Price CC. J Am Chem Soc 1956;78(14):3432–6.
[29] Quirk RP, Lizarraga GM. Macromol Chem Phys 2000;201(13):1395–404.
[30] Billouard C, Carlotti S, Desbois P, Deffieux A. Macromolecules 2004;37(11):4038–43.
[31] Brissault B, Guis C, Cheradame H. Macromolecules 2005;38(20):8244–51.
[32] Lestel L, Cheradame H, Boileau S. Polymer 1990;31(6):1154–8.
[33] Lestel L, Guégan P, Boileau S, Cheradame H, Lauprêtre F. Macromolecules 1992;25(22):6024–8.
[34] Marciniec B. Silicon Chem 2002;1(1):155–75.
[35] Polymer source. In: Technical Data Sheet, Sample P9037-POOCH3. See www.polymersource.com.
[36] Zheng L, Waddon AJ, Farris RJ, Coughlin EB. Macromolecules 2002;35(6):2375–9.
[37] Zheng L, Hong S, Cardoen G, Burgaz E, Gido SP, Coughlin EB. Macromolecules 2004;37(23):8606–11.